.

Assessing Net Growth of Phytoplankton Biomass on Hourly to Annual Timescales Using the Geostationary Ocean Color Instrument.

Joseph E. Salisbury[1], Bror F. Jönsson[2], Antonio Mannino[3], Wonkook Kim[4], Joaquim I. Goes[5], Jin-Yong Choi[6], Javier A. Concha[7]

[1]Ocean Processes Analysis Laboratory, University of New Hampshire, Durham, NH, USA
[2]Plymouth Marine Laboratory, Plymouth, United Kingdom
[3]Ocean Ecology Laboratory, NASA Goddard Space Flight Center, Greenbelt, MD, USA
[4]Department of Civil and Environmental Engineering, Pusan National University, Korea
[5]Department of Marine Biology and Paleoenvironment, Lamont Doherty Earth Observatory at Columbia University, Palisades, New York, USA
[6]Coastal Disaster Research Center, Korea Institute of Ocean Science and Technology, Ansan, Korea
[7]Istituto di Scienze Marine, Consiglio Nazionale delle Ricerche, Rome, Italy

Key Points:

- The Geostationary Ocean Color Instrument tracks changes in net phytoplankton growth at hourly intervals.
- Gains, losses and net accumulations of chlorophyll show strong diurnal and seasonal variability.
- Seasonality in net growth vs light provides evidence for seasonal evolution in phytoplankton community composition.

Corresponding author: Bror Jönsson, brj@pml.ac.uk

Abstract

Questions of whether diurnal changes in carbon fixation affect the global carbon budget cannot be answered using the present generation of polar orbiting ocean color sensors that can only retrieve one image daily. Here we present novel satellite-derived indices of chlorophyll-based production based on the Geostationary Ocean Color Imager (GOCI), whose hourly imaging capability offer the potential for direct estimates of net phytoplankton growth over hourly to seasonal time scales. Our results reveal large variations in net chlorophyll growth in the GOCI study region, both over the day and between seasons. Hourly changes in chlorophyll concentration are highest during spring while growth rates show maxima during the winter. We show seasonal relationships between growth and photon flux. Our study suggests that geostationary ocean color data can be used to constrain phytoplankton productivity on diurnal timescales and be an essential tool to better understand diurnal growth patterns over large spatial regions.

Plain Language Summary

The rate at which microscopic ocean plants, or phytoplankton, consume carbon dioxide represents a gap in scientific knowledge that needs to be filled in order to better model the earth system. To aid in this understanding we use a novel technique that allows us to track the growth behavior of phytoplankton in the Yellow Sea and the East Sea-Japan Sea. This is enabled by using satellite data from the Geostationary Ocean Color Imager, which has the unprecedented ability to collect quality biological information from the ocean surface each daylight hour. We find that the results, while in agreement with local observations and other satellite studies, also contain information about how phytoplankton change over daily to annual cycles and how native communities adapt in response to the annual solar cycle. This information is useful to the ocean modeling community, that seeks to understand various ways in which phytoplankton communities affect the cycling of Earth's carbon.

1 Introduction

The rates at which phytoplankton communities assimilate inorganic carbon, aggregate biomass, and export organic carbon must be determined at at highly resolved spatial and temporal scales in order to understand the ocean's role in the global car-

bon cycle. Such data are critical to advance work in global carbon modeling, and lack of this knowledge presently limits progress in understanding ocean carbon export, transfers of carbon to higher trophic levels and the net air-sea flux of carbon dioxide. Polar orbiting ocean color have been able to provide daily information of phytoplankton biomass with kilometer-scale resolution for several decades and the resulting data fields are used to estimate net primary productivity (NPP) over monthly to decadal time scales (Herman & Platt, 1983; Antoine et al., 1996; Behrenfeld & Falkowski, 1997a; Campbell et al., 2002; Kulk et al., 2020). While satellite derived NPP has been a paradigm shifting resource for our understanding of ocean biology, it continues to be plagued by large uncertainties often in excess of 35% (Behrenfeld & Falkowski, 1997a). Most satellite-based NPP models are based on the concept that Chlorophyll-a (Chl) biomass varies predictably with NPP for a given irradiance (Ryther & Yentsch, 1957; Talling, 1957), scaled by a time-varying photoadaptation parameter (e.g. P_B^{max}, or the maximum daily NPP normalized to biomass). This term is poorly constrained and may represent the largest source of error for satellite-based measurements of NPP limiting their use for ocean carbon and climate studies (Behrenfeld & Falkowski, 1997a, 1997b).

In the past, satellite-derived productivity estimates have been limited by inadequate spatial and temporal coverage of essential parameters (e.g. Photosynthetically Active Radiation (PAR), and Chl) (Maritorena et al., 2010; Feng & Hu, 2016, 2017). Sparse coverage in both time and space necessitates the use of averaging across multi-kilometer scales and over weekly-to-annual intervals. Such averaging is statistically problematic (Lee et al., 2012) since biological growth processes are typically log-normally distributed, which can lead to significant underestimates of the central tendency (Campbell, 1995). As an example, Jönsson and Salisbury (2016) found that within the California Current System, rare events can exert a major influence on mean production estimates made over seasonal time scales, with almost 70 percent of change in biomass driven by only 10 percent of the highest productivity events.

In order to resolve time evolving oceanographic features including phytoplankton dynamics, sediment transport, tracking of pollution and harmful algal events, the Korea Ministry of Oceans and Fisheries designed GOCI, launched June 27th, 2010 (J.-K. Choi et al., 2012; Noh et al., 2018; M. Choi et al., 2019). GOCI provides hourly measurements of ocean color radiance at eight visible/near-infrared spectral bands for wa-

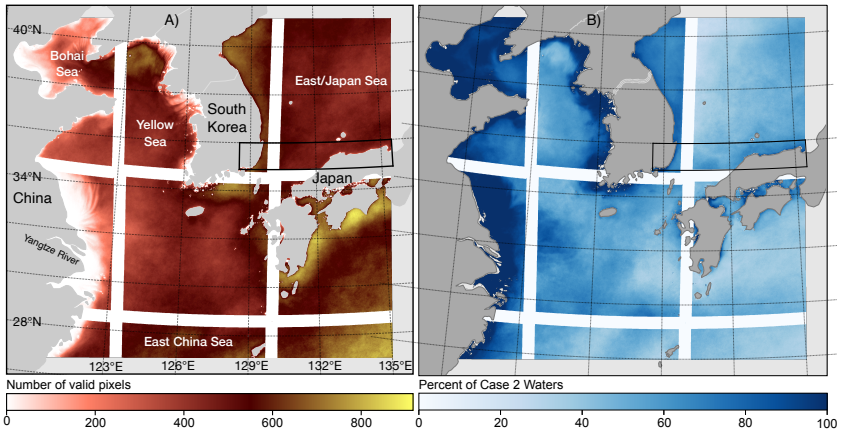

Figure 1. Panel A: Regional extent of the study with available data density (images) for 2016. Any data classified as Case 2 waters (Morel & Prieur, 1977; Lee & Hu, 2006), or where the diffuse attenuation coefficient at 490 nm is higher than 0.2 m^{-1} are masked out to avoid conditions where the primary variation in optical properties is dominated by other properties than Chl. The white grids seen in Figures 1 and 2 are the result of masking out regions influenced by slot effects. The black box encloses an area of detailed study in the East/Japan Sea presented in Figure 4. Panel B: Ratio of values masked as Case 2 waters in percent.

ters in North-East Asia from ∼9:30 am to ∼4:30 pm Korean Standard Time (KST). The hourly repeat cycle significantly increases coverage relative to present polar orbiting ocean color sensors.

The utility of studying phytoplankton communities at high frequencies is obvious as they can be transient on a sub-daily scale (Lohrenz et al., 1988), and phytoplankton populations can double or triple over the course of the day under ideal conditions (Lorenzen, 1963). Thus, GOCI data provides an improved temporal framework to evaluate the diurnal differences in phytoplankton stocks and possibly diurnal variability in photoadaptive parameters (O'Malley et al., 2014).

Here we explore a novel approach to understanding the net growth of phytoplankton that capitalizes on the high temporal measurements of Chl by GOCI. Our investigation centers on analyses of temporal changes in surface ocean Chl biomass as a means to infer net change and growth of phytoplankton over a broad region that

encompasses the clear waters of the Yellow Sea (YS), East China Sea (ECS), and East/Japan Sea (EJS) (Figure 1 panel A). Our goal is to study the regional dynamic behavior of phytoplankton over the course of the illuminated day and document its relationship to diurnal and seasonal changes in PAR.

2 Methods

2.1 GOCI data

GOCI acquires radiometric data hourly over the 2,500 km x 2,500 km area in North East Asia around Korea, which is centered at 130°E 36°N, 8 times per day from 9:30 to 16:30 in local time (UTC+9). GOCI uses a 2-dimensional array that divides the domain into 4-by-4 sub-sections, each of which is called a "slot" (Kang et al., 2010). Data adjacent to these slot boundaries, from 50–100 pixels, exhibit radiometric biases of approximately 2% in top-of-atmosphere radiance for relevant wavebands (Kim et al., 2015). Chl was derived using hourly GOCI L1B data using the recently derived gains (Concha, Mannino, Franz, Bailey, & Kim, 2019; NASA, 2016). The Chl product (OC3, O'Reilly et al., 1998) has an uncertainty of <35% averaged over a range of turbidities (Kim et al., 2016), with uncertainty reduced to ($\pm$1.09 10^{-2} mg m^{-3}) in optically clear waters (Concha, Mannino, Franz, & Kim, 2019). We note that a satellite-derived data set tailored to retrieve the carbon content of phytoplankton may offer additional information to aid in the spatiotemporal accounting of carbon fixed or respired by phytoplankton. However, while such algorithms exist and could be applied to GOCI (e.g. Sathyendranath et al., 2009; Behrenfeld et al., 2005), none have been validated using data from our region of interest, and furthermore, analyses of global data sets show much higher uncertainties for phytoplankton carbon than for satellite-derived Chl (Martínez-Vicente et al., 2017).

The hourly GOCI data were further processed by masking any pixels with solar zenith angles higher than 70° (Gordon, 1990), as consistent with the NASA/L2Gen processing tool (Bailey & Werdell, 2006). We also removed any data that are classified as Case 2 waters (Morel & Prieur, 1977; Lee & Hu, 2006) (Figure 1 panel B), or where the diffuse attenuation coefficient at 490 nm is higher than 0.2 m^{-1} to avoid conditions where the primary variation in optical properties is dominated by other properties than Chl. As recommended in Kim et al. (2015), we also removed all data

within 100 pixels from the slot borders. Hourly instantaneous PAR, (iPAR, μE m^{-2} s^{-1}) estimates derived using GOCI data, based on the algorithm of (Carder et al., 2003), were obtained by special request from the NASA Ocean Biology Processing Group at the Goddard Space Flight Center.

2.2 Hourly changes in Chl

We estimated hourly changes in Chl (ΔChl/Δhr) by calculating Chl$_{t+1}$ – Chl$_t$ element wise in a Eulerian frame for the same day with t time of the day and t+1 one hour later (i.e. 10:30 - 09:30, ..., 16:30 – 15:30). All valid pairs of individual pixels in a subset of the GOCI domain that coincide with the KOOS/MOHID ocean circulation model grid are used in the analysis (see Supplement for model description). A valid pair has Chl values at both time steps. The use of a Eulerian frame to track a local rate of change is potentially problematic since an observed change in Chl can be caused by both local biological processes in the observed water mass and advection of water into the field of view. We tested the use of a Eulerian frame by seeding particles in velocity fields from the KOOS/MOHID, ocean model (Park et al., 2015, and appendix) and then allowed the particles to advect for an hour. The results presented in the supplement (Figure Sup 1) show that particles are advected on average less than 0.25 grid cells over an hour, suggesting that a Eulerian differentiation has a minimal impact on our analyses at hourly time scales. We estimate a specific hourly growth rate of Chl as,

$$\mu_{Chl} = ln\left(\frac{Chl_{t+1}}{Chl_t}\right) \tag{1}$$

with units as hr^{-1}.

While positive values can be expected to reflect a net increase of Chl, it is not the same for negative values. Different physical processes such as vertical mixing, dilution, and vertical settling phytoplankton can all affect the observed concentration of Chl. We believe such processes to not vary significantly over hourly timescales but any negative changes should be interpreted with caution. See Jönsson et al. (2009, 2011) for further discussions.

2.3 Daily changes in Chl

When estimating daily changes in Chl (ΔChl/Δday), however, we must compensate for the contribution to changes in Chl by lateral advection by applying a Lagrangian frame (Jönsson et al., 2009, 2011; Jönsson & Salisbury, 2016). By separating particles seeded at different hours, we generated time series of daily change in Chl staggered in time by using each hourly GOCI determination. This was done by seeding particles evenly, hourly, every day within the context of the KOOS/MOHID ocean circulation model domain, allowing them to advect for two days. Each time a particle position matched with a valid pixel in the GOCI Chl fields, the Chl value reported by GOCI was attached to the particle at its current postion. All pairs of Chl values exactly one day apart were used to calculate a ΔChl/Δday for further analyses. For example, the 09:30 Chl concentration day 2 was subtracted from the 09:30 concentration day 1, the 10:30 concentration day 2 was subtracted from the 10:30 concentration day 1, and so forth. We used data only from March 1 to Nov 30, which represents the time interval with the highest probability for valid GOCI retrievals.

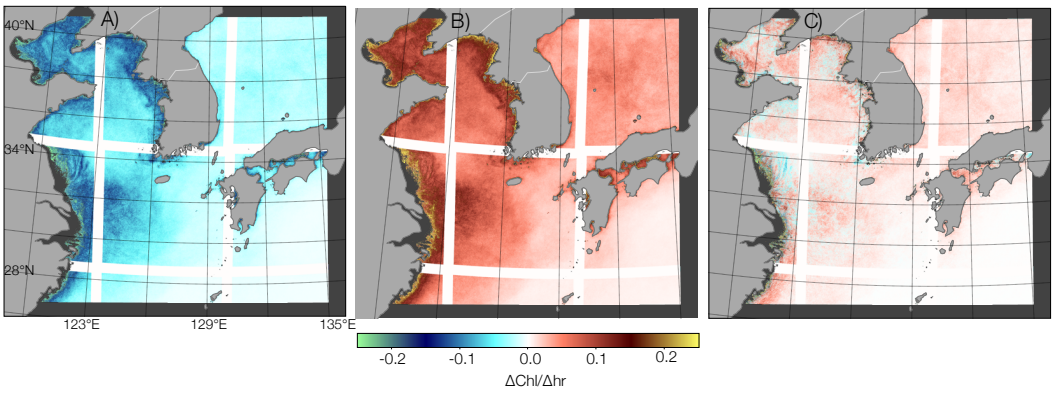

Figure 2. Mapped daily means of ΔChl/Δhr (mg Chl m^{-3} hr^{-1}). The maps are generated by averaging all ΔChl/Δhr values for the full year of 2016 in each grid cell (panel C). Panel A contain only negative values and panel B only positive values. We mask any data that are classified as Case 2 waters, or where the diffuse attenuation coefficient at 490 nm is higher than 0.2 m^{-1}.

3 Results

ΔChl/Δhr data are averaged over the domain and mapped in Figure 2. Dark gray areas within the domain are regions where data failed at least one of the validity tests mentioned in the methods section (Class 2 waters, high, Kd490, high solar angle). The domain is a subset of the full GOCI coverage and selected to cover the KOOS/MOHID ocean model grid. The data show that the magnitudes of both negative and positive values are highest in the coastal regions of the Bohai Sea, YS, and ECS, with the Yangtze Plume showing notably high values. Panel C, analyzed using all data, shows evidence of annual net Chl accumulation (positive average ΔChl/Δhr) throughout most regions. The full dataset of hourly values used to generate Figure 2 is aggregated to a domain-wide daily time series, smoothed by a 30-day running mean and combined in Figure 3. We note that smoothing is for visualization only and is not considered in statistical analyses.

The resulting time series show high positive changes in ΔChl/Δhr during the afternoon during spring and fall, high negative changes during the spring and fall mornings, with much lower amplitudes during the summer. Most of the positive change in Chl occurs after noon, though the 15:30 to 16:30 period shows negative values during summer. Mean daily ΔChl/Δhr is highest in the spring and lowest during the summer (Figure 3).

To assess the relationship between Chl production and light availability, we select a region within the EJS bounded by the coordinates 35°N to 36°N and 127.5°W to 136°W. This is a relatively homogeneous region with ample data and fewer sources of non-biological variability (i.e. river plumes, coastal CDOM). Figure 4 shows a bar plot of average hourly μ_{Chl} against iPAR for each season. The range growth rate values in 0.03 to 0.11h^{-1}, is consistent with other studies of coastal waters (Calbet & Landry, 2004; Li et al., 2010). The relationship between μ_{Chl} and iPAR reveals seasonal variability, with data generally log-normally distributed by season and peaks corresponding differing iPAR values. The seasonal maxima (500 μE m^{-2} s^{-1}, winter; and 1000 μE m^{-2} s^{-1}, spring; 1200 μE m^{-2} s^{-1}, summer and 600 μE m^{-2} s^{-1}, fall).

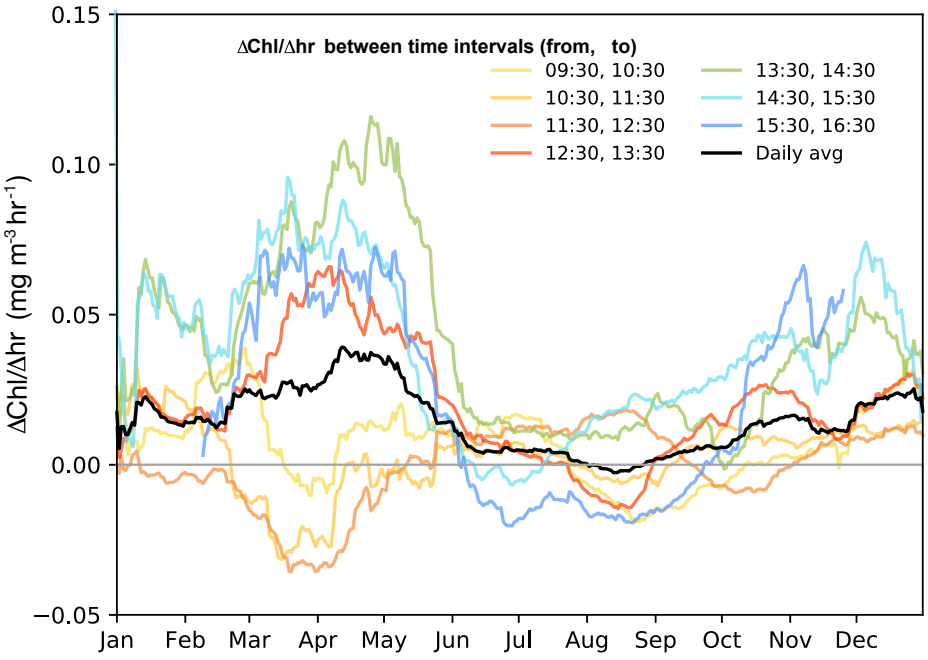

Figure 3. Time series of domain-wide changes in Chl for each hour of GOCI retrievals for the year 2016. The black line shows the mean of all hourly changes plotted for each day.

4 Discussion

This study represents a first attempt to leverage the unique temporal resolution provided by geostationary ocean color satellites to assess biological production in the coastal and open ocean. The combination of hourly temporal and 500-meter spatial resolution enables unprecedented mapping of ΔChl/Δtime and μ_{Chl}, showing large regional and seasonal variability. The observed differences in the seasonal progression of net Chl production (Figures 3 and Sup2) are in line with regional NPP studies (Son et al., 2005; Joo et al., 2015), showing the highest values in spring throughout early summer, albeit with an earlier onset.

These data suggest two notable patterns. First, the magnitude of both the production and loss terms are much higher in spring than in summer or fall, and second, the net productivity versus net losses are not coupled over the course of the day. All determinations from 12:30-13:30 to 15:30-16:30 are positive from Jan to Jun and from Oct to Dec, whereas the morning determinations are most often negative. This pat-

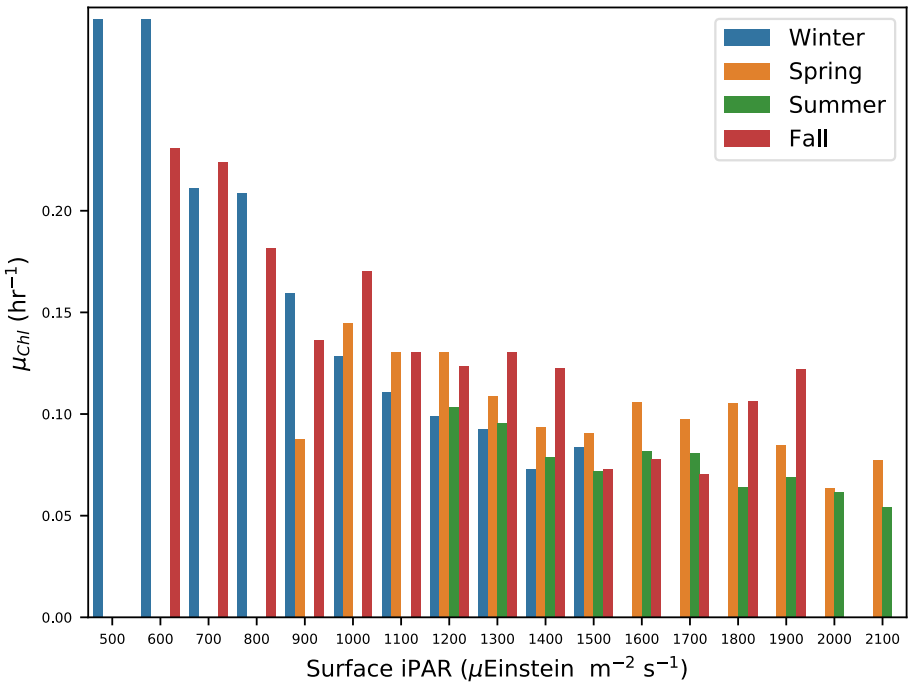

Figure 4. Median Chl-specific growth rate (μ_{Chl}) in iPAR (μE m^2 s^{-1}) bins. Data used is taken from a domain shown in Figure 1 extending from 35°N to 36°N and 127.5°W to 136°W. Seasons are indicated by color (winter, blue), (spring, orange), (summer, green), (fall, red).

tern suggests that the plankton community may be net heterotrophic until noon and that rapid carbon assimilation rates during the morning to early afternoon are required by phytoplankton communities to compensate for night-time respiration (Prézelin & Sweeney, 1977; Bouteiller & Herbland, 1983; Harding et al., 1985; Prézelin, 1992; Schuback & Tortell, 2019) before net Chl accumulation can be observed (Marra, 1997). Interestingly, the net losses of Chl that we observed in the morning appear to parallel the amount of Chl accumulated during the later part of the day. These observations are consistent with those of Mantikci et al. (2017) who noted that magnitudes of respiration are closely related to rates of carbon fixation and the amounts of previously accumulated carbon.

The results presented in Figure 4 suggest that the region hosts at least two physiologically distinct phytoplankton communities, one during winter and fall, and the other during spring and summer, each with different light adaptation. This explana-

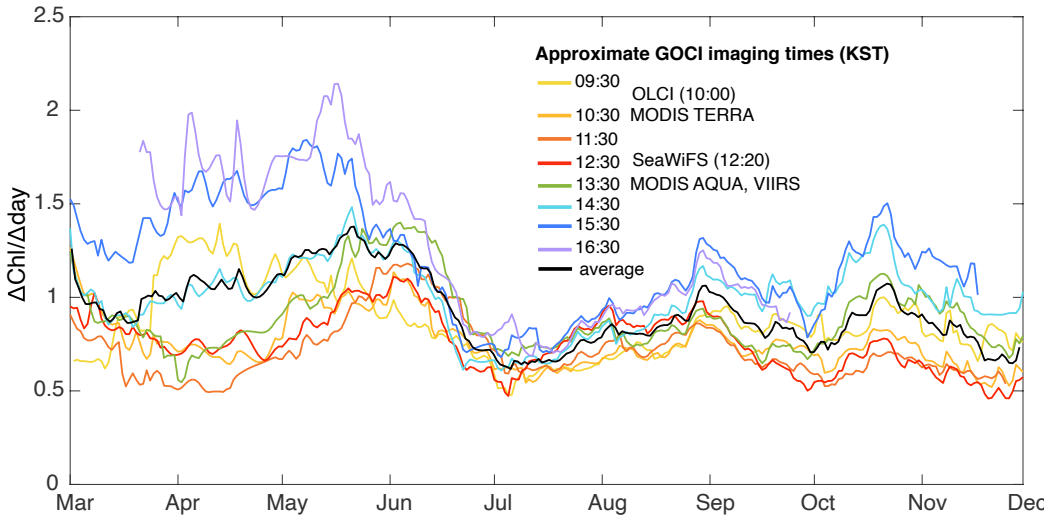

Figure 5. 24-hour Chl differences at each GOCI time step (30-day smoothing applied). Each color shows ΔChl/Δday between different 24-hour intervals based on GOCI imaging times. The black line shows the mean of all hourly changes plotted for each day. The legend also shows equatorial crossing times for various ocean color sensors used to estimate NPP. SeaWiFS (Sea-Viewing Wide Field-of-View Sensor), MODIS (Moderate Resolution Imaging Spectroradiometer; Aqua and Terra refer to different satellites), OLCI (Ocean and Land Color Instrument), VIIRS (Visible Infrared Imaging Radiometer Suite)

tion is consistent with regional studies in temperate waters (Chakraborty et al., 2017; Takahashi et al., 1989), as well as with Joo et al. (2015), whose efforts were focused on the EJS. The fall season shows local maxima for both the 600 μE m^{-2} s^{-1} and the 1000 μE m^{-2} s^{-1} bins. We hypothesize that the high growth rates during the fall at 600-700 μE m^{-2} s^{-1}, indicate a fall bloom of low-light adapted organisms and a rapid switch of the phytoplankton community to adapt to winter light conditions. Alternatively, it is possible our observations are the result single phytoplankton community expressing physiological adaptations to varying light intensities over the seasons. The lack of an observed "ramp up" in Jun-Aug where the lowest light levels show maximum growth rates, suggests that significant low-light production is missing in the analysis. Since the first GOCI image occurs at 09:30, this is likely due to a lack of data earlier in the morning when the photon flux is sufficient to support production. Be-

cause of this, we note that for future geostationary missions, an earlier determination (i.e. 08:30), during the local summer is warranted.

To compare our data with published regional NPP data we examine positive values of ΔChl/Δday based on 24-hour time differences and calculated in a Lagrangian frame (Figure 5). We find these data consistent with seasonal progressions of EJS NPP (e.g. Joo et al., 2015) with similarities that include maxima occurring in May, i.e. the onset of the spring bloom, and the secondary, smaller peaks occurring from September through November. We hypothesize that the domain-averaged time series of positive ΔChl/Δday is a proxy for NPP. This assumption is reasonable if primary production is stochastic and mainly driven by physical events introducing nutrients to the euphotic zone over short timescales (Mahadevan, 2016; Lévy et al., 2012; Jönsson & Salisbury, 2016), and if the response by heterotrophs lags the initiation of primary production to allow phytoplankton to grow over a 24-hr cycle. Alternatively, if ΔChl/Δday remains negative, grazing would be dominant. We conclude thus that positive values would be more representative of NPP and the fact that we see high phytoplankton growth rates (Figure 4) is strongly indicative of heterotrophic grazing being decoupled from phytoplankton growth, and that this is the case. It is clear that ΔChl/Δhr based on GOCI determinations in the afternoon generally suggests a higher NPP than ΔChl/Δday based on determinations from the morning. This difference is of particular concern in the context of NPP estimates based on polar orbiting instruments where at best, only one daily determination is available.

Our assumptions are supported by published values of NPP. Our calculated daily mean changes are in the range between 0.6 and 1.0 mg m^{-3}. By assuming a reasonable carbon to Chl ratio for a productive coastal region of 60 (e.g. Jackson et al., 2017), and integrating the volumetric Chl to the average first optical depth (17m), we estimate median daily phytoplankton C production between April and December to be between 612 and 1275 mg m^{-2} d^{-1}. This is in reasonable agreement with NPP results (632 to 1870 mC m^{-2} d^{-1}) reported for the EJS (Joo et al., 2015; Kwak et al., 2014; Zvalinsky et al., 2019).

Our data suggest that the ΔChl between hours is largely dependent on the integrated photon flux available to stimulate production. For example, the highest average values occur in the afternoon from 14:30 to 16:30, presumably because these later

times allow for the highest integrated photon flux for any given day. Similarly, lower values are usually found earlier in the day. The 24-hour differences are particularly distinct in the 15:30 and 16:30 results seen in Figure 5. We interpret this as indicative of the photon flux needed to overcome a balance of negative values that are observed when differencing between morning values. Put in another way, when 24-hour differences are based on morning values, respiration that dominates in the evening hours drives the balance toward the negative. It is not until later in the day that the integrated photon flux shifts the balance towards positive values. This notion is supported by Noh et al. (2018) who found that in the coastal East Sea, chlorophyll values peaked in the late afternoon. This research also implies that the instant during the day at which an image is captured matters to the overall estimates of productivity. Significant differences in the daily production estimates are observed as different imaging times are used. Figure 5 highlights the differences in NPP that could be estimated from polar orbiting sensors with different equatorial crossing times. Our analyses also highlight the issues of scaling satellite retrieved Chl biomass to NPP, which is the basis for many productivity algorithms (Behrenfeld & Falkowski, 1997b).

Relationships between light absorption and carbon assimilation are often decoupled (Marañón et al., 2003; Schuback & Tortell, 2019), and can change over the daily illumination cycle according to the distribution of PAR and nutrient availability (Falkowski & Raven, 2007). We note that even though our methods provide a robust growth rates based on chlorophyll, we cannot accurately determine physiological variability driving the relative ratios of phytoplankton Chl to carbon. Such work awaits future sensors and the upcoming hyperspectral NASA Plankton, Aerosol, Cloud, Ocean Ecosystem Sensor (PACE), or the NASA Geostationary Littoral Imaging and Monitoring Radiometer (GLIMR), which is also hyperspectral but in a geostationary orbit, should provide improved capabilities for retrieving phytoplankton community composition, fluorescence and particle size and light distributions that could that could lead to advances in understanding phytoplankton physiology from space. We further note that all satellite methods, including ours, presently cannot capture the portion of NPP released as dissolved organic carbon, which accounts for 2-50% of NPP (Thornton, 2014, and references therein). The development of methods that accurately retrieve and track inventories of bioactive constituents over time and space can only serve to improve our understanding of such processes. With robust local algorithms for Chl and rea-

sonable retrieval values for growth rate, our study highlights one aspect of the great potential that geostationary data holds for understanding the variability and magnitude of phytoplankton production.

5 Open Research

Data necessary for generating the results presented in the publication are archived at the Ocean Biology Processing Group, NASA and publicly available (NASA, 2016) under NASA's data policy (`http://science.nasa.gov/earth-science/earth-science-data/data-information-policy/`). Generated data is archived at Zenodo (DOI:10.5281/zenodo.5654874) under the CC BY 4.0 (`https://creativecommons.org/licenses/by/4.0/`) license.

Acknowledgments

We thank everyone involved in the KORUS field campaign for their dedicated service to the study of Geostationary ocean color. This work was in part supported by NASA grants NNX16AD39G (KORUS); 80NSSC21K0563 (Langrangian analyses of ocean color); 80NSSC19M0008 (Geostationary Ocean Color); 80LARC21DA002 – GLIMR 143512; NNH12ZDA001N-ESUSPI (Earth Science U.S. Participating Investigator); GEOCAPE-NNX16AD40G; CMS-80NSSC20K0014. The work was also funded by a Simons Foundation grant (549947, SS) Computational Biogeochemical Modeling of Marine Ecosystems (CBIOMES). We acknowledge instrumental support from the project "Improvements of ocean prediction accuracy using numerical modeling and artificial intelligence technology" funded by the Ministry of Oceans and Fisheries, Korea.

References

Antoine, D., André, J.-M., & Morel, A. (1996). Oceanic primary production: 2. Estimation at global scale from satellite (Coastal Zone Color Scanner) chlorophyll. *Global Biogeochemical Cycles*, *10*(1), 57–69. doi: 10.1029/95gb02832

Bailey, S. W., & Werdell, P. J. (2006). A multi-sensor approach for the on-orbit validation of ocean color satellite data products. *Remote Sensing of Environment*, *102*(1-2), 12–23. doi: 10.1016/j.rse.2006.01.015

Banse, K. (2013). Reflections about chance in my career, and on the top-down regulated world. *Annual Review of Marine Science*, *5*(1), 1–19. doi: 10.1146/annurev

-marine-121211-172359

Behrenfeld, M. J., Boss, E., Siegel, D. A., & Shea, D. M. (2005). Carbon-based ocean productivity and phytoplankton physiology from space. *Global Biogeochemical Cycles*, *19*(1). doi: 10.1029/2004gb002299

Behrenfeld, M. J., & Falkowski, P. G. (1997a). A consumer's guide to phytoplankton primary productivity models. *Limnology and Oceanography*, *42*(7), 1479–1491. doi: 10.4319/lo.1997.42.7.1479

Behrenfeld, M. J., & Falkowski, P. G. (1997b). Photosynthetic rates derived from satellite-based chlorophyll concentration. *Limnology and Oceanography*, *42*(1), 1–20. doi: 10.4319/lo.1997.42.1.0001

Bouteiller, A. L., & Herbland, A. (1983). Diel variation of chlorophyll a as evidenced from a 13-day station in the equatorial Atlantic Ocean. *Deep Sea Research Part B. Oceanographic Literature Review*, *30*(6), 465. doi: 10.1016/0198-0254(83)90227-3

Calbet, A., & Landry, M. R. (2004). Phytoplankton growth, microzooplankton grazing, and carbon cycling in marine systems. *Limnology and Oceanography*, *49*(1), 51–57. doi: 10.4319/lo.2004.49.1.0051

Campbell, J. W. (1995). The lognormal distribution as a model for bio-optical variability in the sea. *Journal of Geophysical Research*, *100*(C7), 13237. doi: 10.1029/95jc00458

Campbell, J. W., Antoine, D., Armstrong, R., Arrigo, K., Balch, W., Barber, R., … Yoder, J. (2002). Comparison of algorithms for estimating ocean primary production from surface chlorophyll, temperature, and irradiance: COMPARISON OF PRIMARY PRODUCTIVITY ALGORITHMS. *Global Biogeochemical Cycles*, *16*(3), 9–1-9-15. doi: 10.1029/2001gb001444

Carder, K. L., Chen, F. R., Lee, Z., Hawes, S. K., & Cannizzaro, J. P. (2003). MODIS ocean science team algorithm theoretical basis document. *ATBD*, *19*(Version 7), 7—18.

Chakraborty, S., Lohrenz, S. E., & Gundersen, K. (2017). Photophysiological and light absorption properties of phytoplankton communities in the river-dominated margin of the northern Gulf of Mexico. *Journal of Geophysical Research: Oceans*, *122*(6), 4922–4938. doi: 10.1002/2016jc012092

Cho, K.-H., Li, Y., Wang, H., Park, K.-S., Choi, J.-Y., Shin, K.-I., & Kwon, J.-I. (2013).

Development and validation of an operational search and rescue modeling system for the yellow sea and the east and south china seas. *Journal of Atmospheric and Oceanic Technology*, *31*(1), 131025110423005. doi: 10.1175/jtech-d-13-00097.1

Choi, J.-K., Park, Y. J., Ahn, J. H., Lim, H.-S., Eom, J., & Ryu, J.-H. (2012). GOCI, the world's first geostationary ocean color observation satellite, for the monitoring of temporal variability in coastal water turbidity: GOCI FOR COASTAL WATER TURBIDITY. *Journal of Geophysical Research: Oceans*, *117*(C9), n/a–n/a. doi: 10.1029/2012jc008046

Choi, M., Lim, H., Kim, J., Lee, S., Eck, T. F., Holben, B. N., ... Saide, P. E. (2019). Validation, comparison, and integration of GOCI, AHI, MODIS, MISR, and VIIRS aerosol optical depth over East Asia during the 2016 KORUS-AQ campaign. *Atmospheric Measurement Techniques Discussions*, 1–31. doi: 10.5194/amt-2019-46

Concha, J., Mannino, A., Franz, B., Bailey, S., & Kim, W. (2019, January). Vicarious calibration of GOCI for the SeaDAS ocean color retrieval. *International Journal of Remote Sensing*, *40*(10), 3984–4001. Retrieved from `https://doi.org/10.1080/01431161.2018.1557793` doi: 10.1080/01431161.2018.1557793

Concha, J., Mannino, A., Franz, B., & Kim, W. (2019, February). Uncertainties in the geostationary ocean color imager (GOCI) remote sensing reflectance for assessing diurnal variability of biogeochemical processes. *Remote Sensing*, *11*(3), 295. Retrieved from `https://doi.org/10.3390/rs11030295` doi: 10.3390/rs11030295

Falkowski, P., & Raven, J. (2007). Photosynthesis and primary production in nature. *Aquatic photosynthesis*, 319—363.

Feng, L., & Hu, C. (2016). Comparison of Valid Ocean Observations Between MODIS Terra and Aqua Over the Global Oceans. *IEEE Transactions on Geoscience and Remote Sensing*, *54*(3), 1575–1585. doi: 10.1109/tgrs.2015.2483500

Feng, L., & Hu, C. (2017). Land adjacency effects on MODIS Aqua top-of-atmosphere radiance in the shortwave infrared: Statistical assessment and correction: LAND ADJACENCY EFFECTS ON MODIS AQUA. *Journal of Geophysical Research: Oceans*, *122*(6), 4802–4818. doi: 10.1002/2017jc012874

Gordon, H. R. (1990). Radiometric considerations for ocean color remote sensors.

Applied Optics, *29*(22), 3228. doi: 10.1364/ao.29.003228

Harding, L., Meeson, B., & Fisher, T. (1985). Photosynthesis patterns in chesapeake bay phytoplankton: short- and long-term responses of p-l curve parameters to light. *Marine Ecology Progress Series*, *26*, 99–111. doi: 10.3354/meps026099

Herman, A. W., & Platt, T. (1983). Numerical modelling of diel carbon production and zooplankton grazing on the Scotian shelf based on observational data. *Ecological Modelling*, *18*(1), 55–72. doi: 10.1016/0304-3800(83)90075-3

Jackson, T., Sathyendranath, S., & Platt, T. (2017). An exact solution for modeling photoacclimation of the carbon-to-chlorophyll ratio in phytoplankton. *Frontiers in Marine Science*, *4*, 283. doi: 10.3389/fmars.2017.00283

Jönsson, B. F., & Salisbury, J. E. (2016). Episodicity in phytoplankton dynamics in a coastal region. *Geophysical Research Letters*, *43*(11), 5821–5828. doi: 10.1002/2016gl068683

Jönsson, B. F., Salisbury, J. E., & Mahadevan, A. (2009). Extending the use and interpretation of ocean satellite data using lagrangian modelling. *International Journal of Remote Sensing*, *30*(13), 3331–3341. doi: 10.1080/01431160802558758

Jönsson, B. F., Salisbury, J. E., & Mahadevan, A. (2011). Large variability in continental shelf production of phytoplankton carbon revealed by satellite. *Biogeosciences*, *8*(5), 1213–1223. doi: 10.5194/bg-8-1213-2011

Joo, H., Son, S., Park, J.-W., Kang, J. J., Jeong, J.-Y., Lee, C. I., … Lee, S. H. (2015). Long-Term Pattern of Primary Productivity in the East/Japan Sea Based on Ocean Color Data Derived from MODIS-Aqua. *Remote Sensing*, *8*(1), 25. doi: 10.3390/rs8010025

Kang, G., Coste, P., Youn, H., Faure, F., & Choi, S. (2010). An In-Orbit Radiometric Calibration Method of the Geostationary Ocean Color Imager. *IEEE Transactions on Geoscience and Remote Sensing*, *48*(12), 4322–4328. doi: 10.1109/tgrs.2010.2050329

Kim, W., Ahn, J.-H., & Park, Y.-J. (2015). Correction of Stray-Light-Driven Interslot Radiometric Discrepancy (ISRD) Present in Radiometric Products of Geostationary Ocean Color Imager (GOCI). *IEEE Transactions on Geoscience and Remote Sensing*, *53*(10), 5458–5472. doi: 10.1109/tgrs.2015.2422831

Kim, W., Moon, J.-E., Park, Y., & Ishizaka, J. (2016). Evaluation of chlorophyll retrievals from geostationary ocean color imager (goci) for the north-

east asian region. *Remote Sensing of Environment*, *184*, 482–495. doi: 10.1016/j.rse.2016.07.031

Kulk, G., Platt, T., Dingle, J., Jackson, T., Jönsson, B. F., Bouman, H. A., … Sathyendranath, S. (2020). Primary Production, an Index of Climate Change in the Ocean: Satellite-Based Estimates over Two Decades. *Remote Sensing*, *12*(5), 826. doi: 10.3390/rs12050826

Kwak, J. H., Lee, S. H., Hwang, J., Suh, Y., Park, H., Chang, K., … Kang, C. (2014). Summer primary productivity and phytoplankton community composition driven by different hydrographic structures in the East/Japan Sea and the Western Subarctic Pacific. *Journal of Geophysical Research: Oceans*, *119*(7), 4505–4519. doi: 10.1002/2014jc009874

Lee, Z., & Hu, C. (2006). Global distribution of Case-1 waters: An analysis from SeaWiFS measurements. *Remote Sensing of Environment*, *101*(2), 270–276. doi: 10.1016/j.rse.2005.11.008

Lee, Z., Jiang, M., Davis, C., Pahlevan, N., Ahn, Y.-H., & Ma, R. (2012). Impact of multiple satellite ocean color samplings in a day on assessing phytoplankton dynamics. *Ocean Science Journal*, *47*(3), 323–329. doi: 10.1007/s12601-012-0031-5

Lévy, M., Iovino, D., Resplandy, L., Klein, P., Madec, G., Tréguier, A. M., … Takahashi, K. (2012). Large-scale impacts of submesoscale dynamics on phytoplankton: Local and remote effects. *Ocean Modelling*, *43-44*, 77–93. doi: 10.1016/j.ocemod.2011.12.003

Li, W. K. W., Lewis, M. R., & Harrison, W. G. (2010). Multiscalarity of the Nutrient–Chlorophyll Relationship in Coastal Phytoplankton. *Estuaries and Coasts*, *33*(2), 440–447. doi: 10.1007/s12237-008-9119-7

Lohrenz, S. E., Wiesenburg, D. A., DePalma, I. P., Johnson, K. S., & Gustafson, D. E. (1988). Interrelationships among primary production, chlorophyll, and environmental conditions in frontal regions of the western Mediterranean Sea. *Deep Sea Research Part A. Oceanographic Research Papers*, *35*(5), 793–810. doi: 10.1016/0198-0149(88)90031-3

Lorenzen, C. J. (1963). DIURNAL VARIATION IN PHOTOSYNTHETIC ACTIVITY OF NATURAL PHYTOPLANKTON POPULATIONS. *Limnology and Oceanography*, *8*(1), 56–62. doi: 10.4319/lo.1963.8.1.0056

Mahadevan, A. (2016). The Impact of Submesoscale Physics on Primary Productivity of Plankton. *Annual Review of Marine Science*, *8*(1), 161–184. doi: 10.1146/annurev-marine-010814-015912

Mantikci, M., Hansen, J. L., & Markager, S. (2017). Photosynthesis enhanced dark respiration in three marine phytoplankton species. *Journal of Experimental Marine Biology and Ecology*, *497*, 188–196. doi: 10.1016/j.jembe.2017.09.015

Marañón, E., Behrenfeld, M., González, N., Mouriño, B., & Zubkov, M. (2003). High variability of primary production in oligotrophic waters of the atlantic ocean: uncoupling from phytoplankton biomass and size structure. *Marine Ecology Progress Series*, *257*, 1–11. doi: 10.3354/meps257001

Maritorena, S., d'Andon, O. H. F., Mangin, A., & Siegel, D. A. (2010). Merged satellite ocean color data products using a bio-optical model: Characteristics, benefits and issues. *Remote Sensing of Environment*, *114*(8), 1791–1804. doi: 10.1016/j.rse.2010.04.002

Marra, J. (1997). Analysis of diel variability in chlorophyll fluorescence. *Journal of Marine Research*, *55*(4), 767–784. doi: 10.1357/0022240973224274

Martínez-Vicente, V., Evers-King, H., Roy, S., Kostadinov, T. S., Tarran, G. A., Graff, J. R., … Sathyendranath, S. (2017). Intercomparison of Ocean Color Algorithms for Picophytoplankton Carbon in the Ocean. *Frontiers in Marine Science*, *4*, 378. doi: 10.3389/fmars.2017.00378

Morel, A., & Prieur, L. (1977). Analysis of variations in ocean color1: Ocean color analysis. *Limnology and Oceanography*, *22*(4), 709–722. doi: 10.4319/lo.1977.22.4.0709

NASA, O. B. P. G. (2016). GOCI Level 2 Ocean Color Data Version 2014. *website*. Retrieved from `http://oceancolor.gsfc.nasa.gov/data/10.5067/COMS/GOCI/L2/OC/2014` doi: 10.5067/coms/goci/l2/oc/2014

Noh, J. H., Kim, W., Son, S. H., Ahn, J.-H., & Park, Y.-J. (2018). Remote quantification of cochlodinium polykrikoides blooms occurring in the East Sea using geostationary ocean color imager (GOCI). *Harmful Algae*, *73*, 129–137. doi: 10.1016/j.hal.2018.02.006

O'Malley, R. T., Behrenfeld, M. J., Westberry, T. K., Milligan, A. J., Shang, S., & Yan, J. (2014). Geostationary satellite observations of dynamic phytoplankton photophysiology. *Geophysical Research Letters*, *41*(14), 5052–5059. doi:

10.1002/2014gl060246

O'Reilly, J. E., Maritorena, S., Mitchell, B. G., Siegel, D. A., Carder, K. L., Garver, S. A., ... McClain, C. (1998). Ocean color chlorophyll algorithms for SeaWiFS. *Journal of Geophysical Research: Oceans*, *103*(C11), 24937–24953. doi: 10.1029/98jc02160

Park, K.-S., Heo, K.-Y., Jun, K., Kwon, J.-I., Kim, J., Choi, J.-Y., ... Jeong, S.-H. (2015). Development of the Operational Oceanographic System of Korea. *Ocean Science Journal*, *50*(2), 353–369. doi: 10.1007/s12601-015-0033-1

Prézelin, B. B. (1992, Jan). Diel periodicity in phytoplankton productivity. In T. Berman, H. J. Gons, & L. R. Mur (Eds.), (pp. 1–35). Springer Netherlands. Retrieved from `https://doi.org/10.1007/978-94-011-2805-6_1` doi: 10.1007/978-94-011-2805-6_1

Prézelin, B. B., & Sweeney, B. M. (1977). Characterization of photosynthetic rhythms in marine dinoflagellates: Ii. photosynthesis-irradiance curves and in vivo chlorophyll a fluorescence. *Plant Physiology*, *60*(3), 388–392. doi: 10.1104/pp.60.3.388

Ryther, J. H., & Yentsch, C. S. (1957). The Estimation of Phytoplankton Production in the Ocean from Chlorophyll and Light Data1. *Limnology and Oceanography*, *2*(3), 281–286. doi: 10.1002/lno.1957.2.3.0281

Sathyendranath, S., Stuart, V., Nair, A., Oka, K., Nakane, T., Bouman, H., ... Platt, T. (2009). Carbon-to-chlorophyll ratio and growth rate of phytoplankton in the sea. *Marine Ecology Progress Series*, *383*, 73–84. doi: 10.3354/meps07998

Schuback, N., & Tortell, P. D. (2019). Diurnal regulation of photosynthetic light absorption, electron transport and carbon fixation in two contrasting oceanic environments. *Biogeosciences*, *16*(7), 1381–1399. doi: 10.5194/bg-16-1381-2019

Son, S., Campbell, J., Dowell, M., Yoo, S., & Noh, J. (2005). Primary production in the Yellow Sea determined by ocean color remote sensing. *Marine Ecology Progress Series*, *303*, 91–103. doi: 10.3354/meps303091

Takahashi, M., Ichimura, S., Kishino, M., & Okami, N. (1989). Shade and chromatic adaptation of phytoplankton photosynthesis in a thermally stratified sea. *Marine Biology*, *100*(3), 401–409. doi: 10.1007/bf00391156

Talling, J. F. (1957). THE PHYTOPLANKTON POPULATION AS A COMPOUND PHOTOSYNTHETIC SYSTEM*. *New Phytologist*, *56*(2), 133–149. doi: 10.1111/

j.1469-8137.1957.tb06962.x

Thornton, D. C. (2014). Dissolved organic matter (DOM) release by phytoplankton in the contemporary and future ocean. *European Journal of Phycology*, *49*(1), 20–46. doi: 10.1080/09670262.2013.875596

Zvalinsky, V. I., Lobanova, P. V., Tishchenko, P. Y., & Lobanov, V. B. (2019). Estimation of Primary Production in the Northwestern Part of the Sea of Japan by Ship- and Satellite-Based Observations. *Oceanology*, *59*(1), 37–48. doi: 10.1134/s0001437019010223